Estimation of Static Energy Meter Interference in Waveforms Obtained in On-Site Scenarios

Bas ten Have, *Student Member, IEEE*, Marco A. Azpúrua, *Senior Member, IEEE*, Tom Hartman, *Student Member, IEEE*, Marc Pous, *Member, IEEE*, Niek Moonen, *Member, IEEE*, Ferran Silva, *Senior Member, IEEE*, and Frank Leferink, *Fellow, IEEE*

***Abstract*—Static energy meters have shown errors beyond the standards due to conducted electromagnetic interference of pulsed currents. This was observed in several case studies and confirmed by laboratory experiments, which showed errors up to 2675%. The extent of this interference case is unknown, because there is limited information about the waveforms occurring in the real on-site scenarios. This article aims to detect critical waveforms in on-site surveyed data that have similar characteristics as the pulses that resulted in metering errors. The time-domain parameters of the laboratory experiments that show static energy meter interference are compared to the on-site waveform data using an interpolation based on an inverse weighting distance function. Using this approach, the waveform characteristics are compared, and an error is estimated. This approach was satisfactorily validated using data from validation experiments that shows a correct estimation of the actual error according to the permissible limits for energy metering for all validation indices. The performed on-site surveys show the existence of nonlinear waveforms. During the survey of three sites for ten days, 19 531 waveforms were captured, of which 14 487 indicate large nonlinearities and 379 are estimated to produce metering errors up to 925%.**

***Index Terms*—Electromagnetic interference (EMI), nonlinear waveforms, on-site survey, static energy meters, time domain.**

I. Introduction

STATIC energy meters measure the energy consumption in residential situations for billing purposes. In previous research, major interference errors of a number of specimens of static energy meters are shown in diverse test conditions. The interference was observed due to harmonic disturbances [1], photovoltaic (PV) installations and power drive systems [2]–[4], and active in-feed converters [5], which, possibly combined with a higher number of complaints and failures, resulted in faster publication of the CLC/TR50579 [6] technical report and IEC 61000-4-19 standard [7]. In more recent studies, errors have been found resulting from conducted electromagnetic interference (EMI) of dimmed lighting equipment, light-emitting diode and compact fluorescent lighting technology [8]–[10], and a speed-controlled water pump [11], [12]. In [11], maximum experimental errors of 2675% are found. The corresponding drawn currents are nonlinear pulsed currents with a high peak amplitude and a low root mean square (RMS) value. In [13], static energy meter errors are found due to undershoot and overshoot effects of the integrated circuit technology when using pulsed currents.

TABLE I
Critical Ranges of Time-Domain Parameters Found to Result in Interference of Static Energy Meters [14]

Parameter	Critical range
Charge	4-8 mC
Crest factor	> 5
Pulse width	0.2-1.2 ms
Rising slope	> 0.1 A/μs

A parametric model that provides a simplified description of such drawn complex nonlinear currents is developed in [14]. This model shows that the interference currents are narrow fast rising pulses, where a higher crest factor, narrower pulsewidth, less charge, and a higher slope are the factors that contribute most to an increase in the interference. The critical ranges of these time-domain parameters are shown in Table I.

The extent of the interference cases involving static energy meters is unknown because there is limited information about the waveforms drawn in household situations. Therefore, it is of interest to indicate the occurrence of similar pulsed waveforms resulting in interference in real situations. In [15], the existence of current waveforms with fast inclining slopes that occur in low-voltage (LV) customer terminals is shown. Moreover, within the framework of the MeterEMI project [16], surveys are performed in modern LV networks, including networks with electric vehicle (EV) charging stations [17], and PV installations [18]. It was found that the on-site surveyed waveforms are typically a superposition of the fundamental frequency, other frequency components including pulses, and low-amplitude random noise. This makes it complex to analyze the parameters of the pulses

Manuscript received March 29, 2021; revised May 10, 2021; accepted June 9, 2021. Date of publication July 12, 2021; date of current version February 17, 2022. This project 17NRM02 MeterEMI was supported in part by the EMPIR program co-financed by the Participating States and in part by the European Union's Horizon 2020 research and innovation program. *(Corresponding author: Bas ten Have.)*

Bas ten Have, Tom Hartman, and Niek Moonen are with the University of Twente, 7522 Enschede, The Netherlands (e-mail: bas.tenhave@utwente.nl; tom.hartman@utwente.nl; niek.moonen@utwente.nl).

Frank Leferink is with the University of Twente, 7522 Enschede, The Netherlands, and also with Thales Nederland B.V., 7550 Hengelo, The Netherlands (e-mail: leferink@ieee.org).

Marco A. Azpúrua, Marc Pous, and Ferran Silva are with the Universitat Politécnica de Catalunya, 08034 Barcelona, Spain (e-mail: marco.azpurua@upc.edu; marc.pous@upc.edu; ferran.silva@upc.edu).

Color versions of one or more figures in this article are available at https://doi.org/10.1109/TEMC.2021.3089877.

Digital Object Identifier 10.1109/TEMC.2021.3089877

included in such signals and to correlate them to static energy meter interference.

Therefore, this article aims to detect the critical current waveforms in relation to interference of metering errors that occur in a large set of on-site surveyed data. This is achieved by comparing the on-site waveforms with a reference dataset, including the parameters that were found to be critical in laboratory experiments. For this purpose, the on-site waveforms with an unknown metering error are processed to extract their relevant waveform parameters, and then, the interference is estimated using an interpolation function. This provides a tool for objectively and automatically selecting those on-site waveforms with similar time-domain characteristics as those from the reference dataset. Considering that similar critical waveforms result in comparable mean errors, this approach is expected to effectively identify which of such surveyed waveforms could induce static energy meter interference.

The rest of this article is organized as follows. Section II describes the parametric waveform model for the characterization of pulses in on-site waveforms. Section III describes and validates the approach to estimate the interference. Section IV describes the measurement method used to survey on-site current waveforms. In Section V, the results of the survey are presented, showing a statistical overview of the parameters encountered at the on-site and the estimated static energy meter errors of such waveforms based on the introduced estimator. Then, Section VI discusses these findings. Finally, Section VII concludes this article.

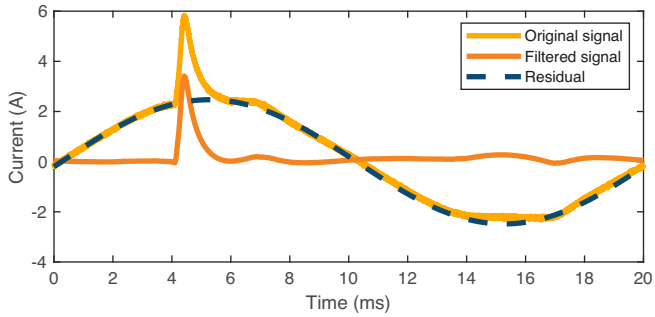

Fig. 1. Mains frequency filter separating the pulsed part from the fundamental frequency of a measured signal.

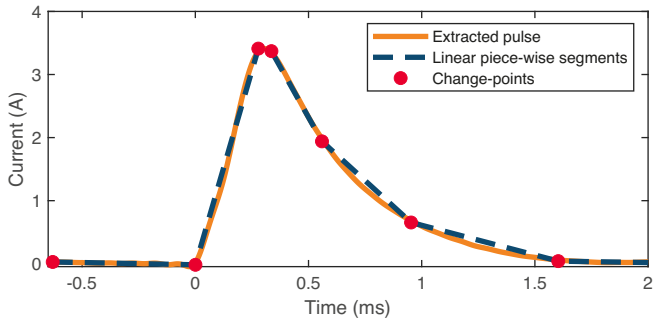

Fig. 2. Extracted pulse and modeled waveform resulting from a pulsed time-domain current.

II. Parametric Waveform Model for the Characterization of Pulses in On-Site Waveforms

The waveforms measured in on-site situations are a superposition of different signals consisting of a combination of linear (resistive) and nonlinear loads, and noise. The aim of this model is to characterize the pulsed part of such waveforms in a simplified manner, as the pulsed parts are correlated with static energy meter interference in [14]. Therefore, in postprocessing, the pulsed and linear parts are separated using a mains frequency filter, after which the time-domain characteristics are determined using a parametric waveform model introduced in [14]. The filter makes the model more robust to noise as well as to the presence of nonimpulsive current components.

A. Filtering out the Mains Frequency

The mains (fundamental) frequency is removed from the measured signal, because it does not cause metering errors, and it simplifies the waveform by retaining the pulsed part that could be correlated with the interference. The spectrum of the waveform is calculated using a fast Fourier transform, after which the frequency contents between 40 and 60 Hz are removed, such that higher order harmonics remain unchanged. Fig. 1 shows an example of a test wave that consists of a harmonic-distorted sine wave superposed with a pulse. After applying the mains frequency filter, the pulse is separated from the fundamental frequency.

B. Parametric Waveform Model

The parametric waveform model in [14], which describes the time-domain characteristics of a pulsed waveform, can now be applied. It indicates change points at the extreme points of the waveform where the statistical properties change and fits linear piecewise segments in between. An optimal number of ten change points was found in [14] that preserve the shape of the original waveform while reducing its complexity. Consequently, noise will not be treated as a statistical change, so the model is robust against low-amplitude random noise present in the waveform. The filtered signal in Fig. 1 is modeled using this approach resulting in Fig. 2, which forms a fair representation of the original pulse. The use of this model is needed because conventional tools determine time-domain parameters based on bilevel pulses, which is not the case for the waveforms encountered on-site. For example, Fig. 3 shows a pulse with more than two levels, due to oscillations in realistic waveforms.

Then, a set of scalar parameters is obtained to describe the pulsed part of the waveform in the time domain. Instead of using the pulsewidth (t_{width}), defined as the time the signal needs in between its rise to 50% and its fall to 50% of the peak value [19], another metric is used for the duration of a pulse. Because waveforms are encountered which are a superposition of two consecutive pulses where the first pulse has a relatively large amplitude compared to the second one, as it is exemplified in Fig. 3. The pulsewidth will only relate to the first part of the pulse because the amplitude of the second part is lower than the

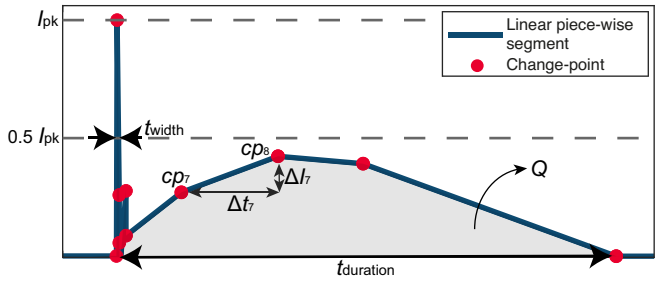

Fig. 3. Parametric description of a modeled waveform.

50% reference threshold. Choosing a different threshold level for measuring the pulsewidth would not work due to the slow decaying feature of the later part of the waveform. Therefore, pulse duration is defined as the time between the start and end instants of the pulse, which could easily be determined using the modeled pulse, as a change point is provided at the start and end of the pulse. The modeled pulse is described by the following set of scalar parameters, which are exemplified in Fig. 3 and explained in more detail in [14]:

1) charge (Q): the area circumferenced by the pulse and the zero current line;
2) crest factor (CF): the ratio between the peak value (I_{pk}) and the RMS value (I_{rms}) of the pulse;
3) maximum slope ($\Delta I/\Delta t$): the maximum slope between two consecutive change points;
4) peak value (I_{pk}): the peak value of the pulse;
5) pulse duration (t_{duration}): the time between the start and end instants of the modeled pulse.

III. Estimation of the Static Energy Meter Errors

An estimator is created to select critical waveforms from a large set of waveforms recorded on-site. The estimator is based on a reference dataset of laboratory experiments, of which the static energy meter errors are accurately known. The waveforms included in the dataset are characterized using the scalar parameters described in Section II. Then, for on-site recorded waveforms, of which the static energy meter deviations are unknown, the scalar parameters are determined and interpolated to this dataset using an inverse distance weighting (IDW) function resulting in an estimated error.

A. Description of the Reference Dataset

The dataset contains 138 laboratory experiments, of which the static energy meter deviations are known. It consists of 60 experiments that were published earlier in [10]–[12] and 24 experiments with slightly varied measurement conditions. In most of these 84 experiments, static energy meter errors were observed. Furthermore, the dataset comprises 54 experiments that did not induce metering errors. These mostly include linear waveforms or pulses with less extreme parameters. All of these 138 waveforms, $p_n(t)$, have a set of parameters, $\mathbf{S}_n$. Interparameter dependencies are shown in [14], i.e., different parameters show similar correlations with static energy meter errors; therefore, the peak value and charge are not included in this model to avoid redundancy. The dataset is described by

$$\mathbf{S}_n = \left\{ CF_n; \frac{\Delta I_n}{\Delta t}; t_{\text{duration,n}} \right\} (p_n(t)) \tag{1}$$

and a corresponding measured static energy meter error, e_n. Here, the errors are determined using

$$e_n\,[\%] = \frac{P_{\text{SM}} - P_{\text{ref}}}{P_{\text{ref}}} \cdot 100\% \tag{2}$$

where P_{SM} is the power measured by the static energy meter under test and P_{ref} is the power of the reference power analyzer, according to the measurement procedure explained in [10]–[12]. From the ten selected specimens of static energy meters, it was observed that not all result in the same magnitude of errors. Therefore, the estimator will be referred to the worst case, as the maximum error represents the most critical interference case.

B. IDW Function

For the estimation of static energy meter interference of waveforms, from which the errors are unknown, it is assumed that similar waveforms will result in similar interference. In this regard, similar waveforms are those characterized by parameters that are close to each other in terms of their Euclidean distance. Therefore, it is reasonable to assume that an unknown waveform, $p_u(t)$, having a set of parameters, $\mathbf{S}_u$,

$$\mathbf{S}_u = \left\{ CF_u; \frac{\Delta I_u}{\Delta t}; t_{\text{duration,u}} \right\} (p_u(t)) \tag{3}$$

will result in a metering error e_u that can be estimated through an interpolation function, i.e., $\tilde{e}_u = f(\mathbf{S}_u)$. In this regard, a suitable alternative for the interpolation method is the IDW function [20]. Because the dataset interpolates the parameters to the static energy meter errors, $\{\mathbf{S}_1, \mathbf{S}_2, \ldots, \mathbf{S}_{138}\} \rightarrow \{e_1, e_2, \ldots, e_{138}\}$, according to a deterministic relationship and also because the points in the dataset are scattered in the study region. And thus weights the similarities between the parameters of the interpolated (unknown) waveforms with the reference dataset indirectly. Accordingly, we have

$$f(\mathbf{S}_u) = \begin{cases} \dfrac{\sum_{n=1}^{N} w_n(\mathbf{S}_u) e_n}{\sum_{n=1}^{N} w_n(\mathbf{S}_u)}, & \text{if } d(\mathbf{S}_u, \mathbf{S}_n) \neq 0 \; \forall \; n \\ e_n, & \text{if } \exists \; n \in d(\mathbf{S}_u, \mathbf{S}_n) = 0 \end{cases} \tag{4}$$

where the weighting function, $w_n(\mathbf{S}_u)$, is

$$w_n(\mathbf{S}_u) = \frac{1}{d(\mathbf{S}_u, \mathbf{S}_u)^{\alpha}} \tag{5}$$

d is the metric operator (in this case the Euclidean distance) and α is the power parameter. The above equations indicate that the weight decreases as the distance increases from the interpolated points. Moreover, greater values of α assign greater influence to values closest to the interpolated point. A power parameter value of 4 is found to provide a good fit between the reference dataset and the validation experiments provided in Section III-C.

TABLE II
TIME-DOMAIN PARAMETERS, ESTIMATED (E_{EST}), AND REAL ERROR (E_{REAL}) OF THE VALIDATION MEASUREMENTS

	Negative error					No error					Positive error									
Index	1	2	3	4	5	6	7	8	9	10	11	12	13	14	15	16	17	18	19	20
Q (mC)	3.3	3.0	4.5	5.2	5.5	0.2	11.4	4.6	4.1	2.6	2.8	5.3	3.3	7.1	6.4	4.1	6.2	7.2	7.1	3.8
CF	29	29	19	24	21	4	3	3	3	3	7	7	7	6	6	8	6	6	8	11
$\Delta I/\Delta t$ (A/µs)	9.0	8.4	9.3	8.4	8.7	0.01	0.02	0.03	0.08	0.01	0.3	0.9	1.3	1.1	0.9	0.9	0.9	0.6	0.4	0.6
I_{pk} (A)	18	18	17	20	20	0.2	2	2	2	2	12	15	10	15	15	12	14	15	16	19
$t_{duration}$ (ms)	0.9	1.0	0.9	1.8	1.8	7.9	5.3	3.9	18.3	1.8	3.0	0.8	2.6	0.9	0.9	0.7	0.9	0.9	1.0	0.4
e_{est} (%)	-76	-74	-36	-28	-9	0	0	0	0	0	78	143	188	199	203	212	214	229	331	1608
e_{real} (%)	-64	-30	-10	-26	-18	-2	1	-1	-2	0	28	239	183	301	276	266	304	211	331	1087

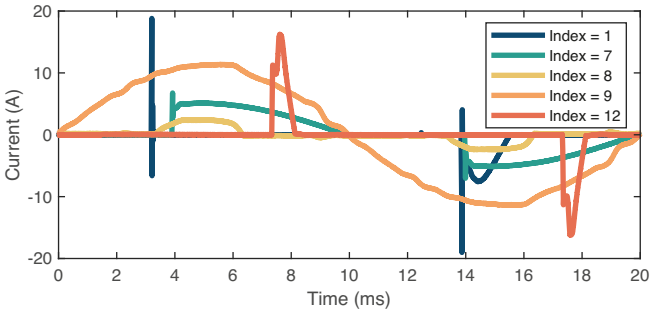

Fig. 4. Waveforms of the validation measurements.

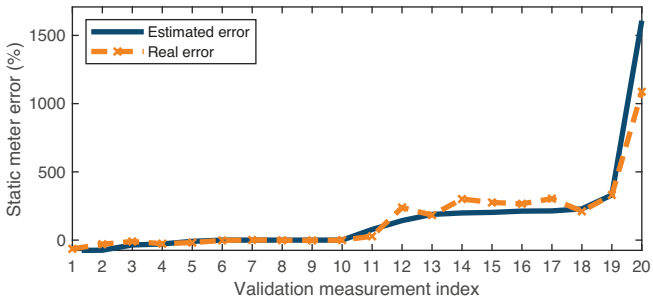

Fig. 5. Estimated and real errors of the validation experiments.

This translates into an appropriate neighboring region for interpolating the unknown waveforms and a reasonable importance of outliers.

C. Validation of the Error Estimator

Twenty experiments that are not included in the reference dataset are used to validate the accuracy of the estimator. The experiments are performed using the same methodology as the data in the reference dataset. Five cases with negative errors (index = 1–5), five cases with no error outside the limits for electricity meters [21] (index = 6–10), and ten cases with positive errors (index = 11–20) are included. The associated waveforms for indices 1, 6, 8, 9, and 12 are visualized in Fig. 4, and Table II shows the parameters. These wave shapes repeat every mains cycle during the whole measurement period. The waveforms resulting in a negative error all have a similar shape as the waveform with index 1; however, there is a slight difference in the parameters. It is remarkable that all those waveforms have a sharp transient that contains almost no charge in the positive part of the fundamental voltage (as the voltage is in phase with the waveform with index 9). The waveforms resulting in no error show a chopped sinusoidal waveform (indices 6 and 7), a relatively wide pulse with a low peak value (indices 8 and 10), or a clear sinusoidal waveform (index 9). The waveforms resulting in a positive error all have a similar shape as index 12, but with slightly different parameters, which affects the magnitude of the error. The estimated and real errors are presented in Fig. 5 and Table II. The estimator matches the real errors reasonably well, as for all indices, it was correctly estimated if the error was negative, nonexisting, or positive. This is, thus, a valuable tool for selecting critical waveforms from a large set of on-site captured data, after which more concise and precise measurements can be performed effectively.

IV. METHOD FOR ON-SITE SURVEY

To indicate the existence of pulsed currents that could interfere with static energy meters in on-site situations, a survey is conducted. Three different test sites are surveyed, which consists of an industrial plant using EV charging stations in Viladecavalls (Barcelona), Spain (site 1), a consumer residence that includes PV installation in Gelida (Barcelona), Spain (site 2), and an apartment in Enschede, The Netherlands (site 3). Site 1 uses a three-phase system, while sites 2 and 3 use a single-phase system. Some preliminary results of sites 1 and 2 were already published in [17] and [18].

A. Measurement Setup

Measurements are performed at the meter connection point, to measure the complete residential system, and thus the signals to which installed static energy meters are exposed to. During the measurement survey, it was not known which appliances were turned ON. For the three-phase system (site 1), the currents on all three lines (L1, L2, and L3) were measured; for the single-phase systems (sites 2 and 3), the current on the line and the neutral conductor was measured. The current is measured using flexible current probe model TA325 from Pico Technology and is within

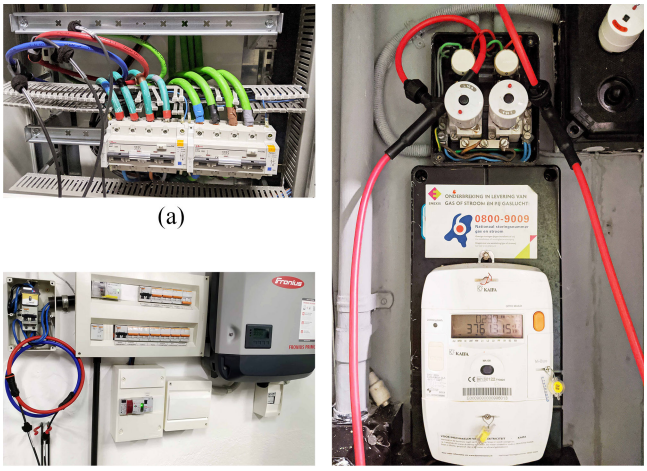

Fig. 6. Installed measurement setup at the consumers' meter connection point. (a) Site 1. (b) Site 2. (c) Site 3.

0.5-dB accuracy in the frequency range up to 20 kHz, calibrated according to [22], where it was also verified that the probe's response time was sufficient to measure fast changing pulsed currents without major influences on the measured waveform. The transducers are connected to a 5444B Picoscope digitizer from the same manufacturer. Time-domain EMI measurement and processing system software [23] is controlling the digitizer via a laptop. Fig. 6 shows the installed measurement setup at the consumers' meter connection point.

B. Measurement Settings

The current waveforms were monitored during an interval of ten days. The acquired waveforms were analyzed in order to preselect and store meaningful data only. For that purpose, specific triggering settings were used based upon the pulsed waveforms of interest following the procedure in [18], which are amplitude probability distribution (APD) and discrete wavelet transform, which are strong indicators for pulsed waveforms [24], [25]. Furthermore, snapshots (instantaneous acquisitions) are made every 10 min. In this way, a representative set of waveforms (events) in the surveyed sites is gathered. The measurement time for each triggered acquisition was ten cycles at mains frequency (50 Hz), which is equivalent to 200 ms. The waveform sampling rate was set to 1 MS/s.

V. Results Obtained From On-Site Survey

The time-domain parameters are extracted from on-site surveyed waveforms and are presented statistically in Fig. 7, using the Turkey's boxplot method [26]. Points with a value of 1.5 times the interquartile range from the median are marked as outliers and are visible with a dot. The value of the median (Q2), lower (Q1) and upper (Q3) quartile, and the minimum (min) and maximum (max) are presented in the graph. The range in which parameters are found to be critical in relation to static energy meter errors, according to Table I, is indicated in red. For the peak value, no critical range is included, as this

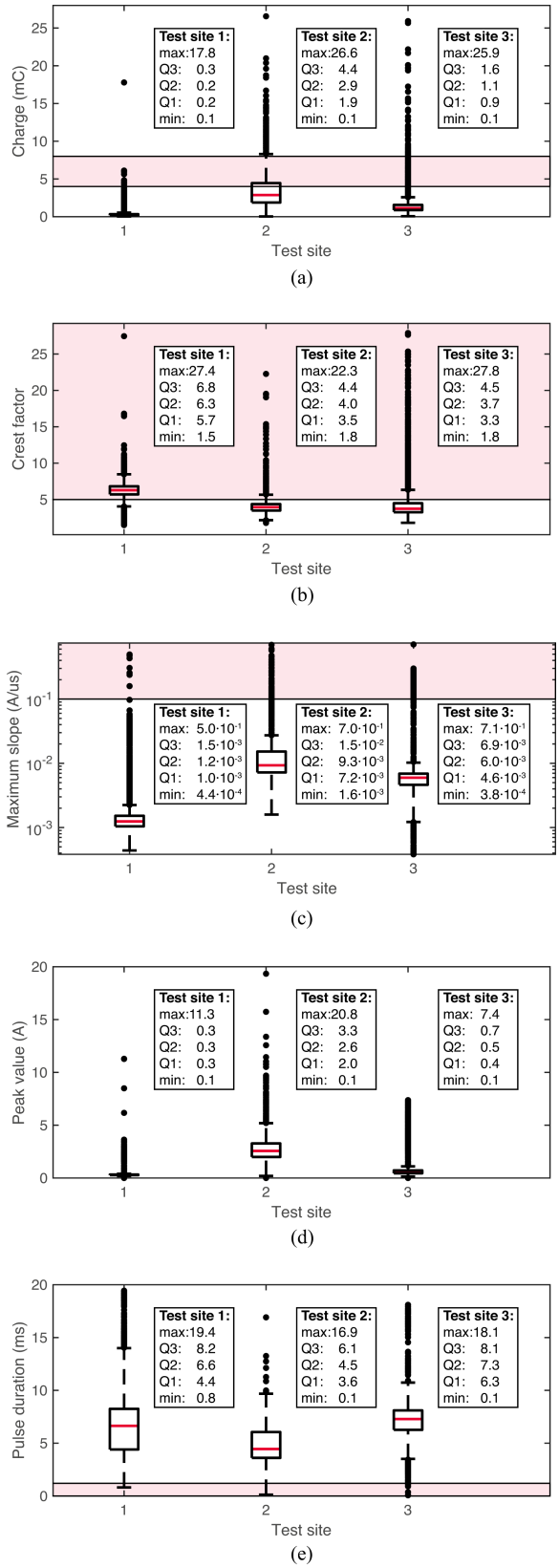

Fig. 7. Statistical overview of the time-domain parameters that occurred in the three surveyed test sites. (a) Charge. (b) Crest factor. (c) Maximum slope. (d) Peak value. (e) Pulse duration.

TABLE III
OVERVIEW OF ON-SITE SURVEY, SHOWING THE CAPTURED EVENTS, EVENTS CONTAINING CRITICAL PARAMETERS, AND EVENTS HAVING ESTIMATED ERRORS

Site	Events	Critical parameters	Estimated errors
1	14295	13304	3
2	1230	404	44
3	4006	779	332

parameter on itself does not correlate with meter readings, e.g., a large value could relate to a large pulse but also to a linear waveform with high peak value. However, the charge and peak value are not included in the estimator; those are provided here for a complete statistical overview of the waveforms. The graph shows the typical ranges of the parameters and their variability. In 74% of the captured events, at least one parameter was inside the critical area of static energy meter errors. An overview of the captured events, the events containing at least one critical parameters, and the events where a static energy meter error is estimated is provided in Table III. These are explained per test site hereafter.

A. Test Site 1

For site 1, the APD trigger captured a large number of low-amplitude noisy waveforms, which explains the considerably higher number of triggered events compared to the other sites. Consequently, the crest factor is inside the critical red area and explains the 13 304 events with a critical parameter. However, these pulses have a low charge, slope, and peak value; furthermore, the pulse duration is large. Still, for the three events, an error is estimated, which is 19%, 86%, and 333%, respectively. The corresponding waveforms are distorted sinusoidal, as shown in Fig. 8(a). The wave shape repeats for multiple consecutive cycles as long as the source of interference is turned ON. The extremity of the waveforms' rising slope determines the magnitude of the error . No pattern was recognized in the occurrence of these events containing estimated errors, so these peaks occur seemingly at random. Such pulse indicates an inrush current from the connected equipment.

B. Test Site 2

In site 2, 1230 events are captured, of which a third of them (32.8%) contain critical parameters. The pulses contain more charge and have a higher peak value compared to site 1. For 44 events, an error is estimated, mostly because of fast rising slopes combined with a high crest factor. Fig. 8(b) shows an example waveform, for which an error is estimated; it shows a pulse that is present in a distorted sinusoidal waveform, which repeats for multiple consecutive cycles. The other waveforms, of which errors are estimated, contain similar pulses, and the extremity of the time-domain parameters, such as combination of the crest factor, maximum slope, and pulse duration, determines the magnitude of the error. The estimated errors range from −29% to 464%, where the highest estimated interference corresponds to the most extreme combination of the time-domain parameters. Similar to site 1, these pulses occur seemingly at random as there is no pattern in its occurrence.

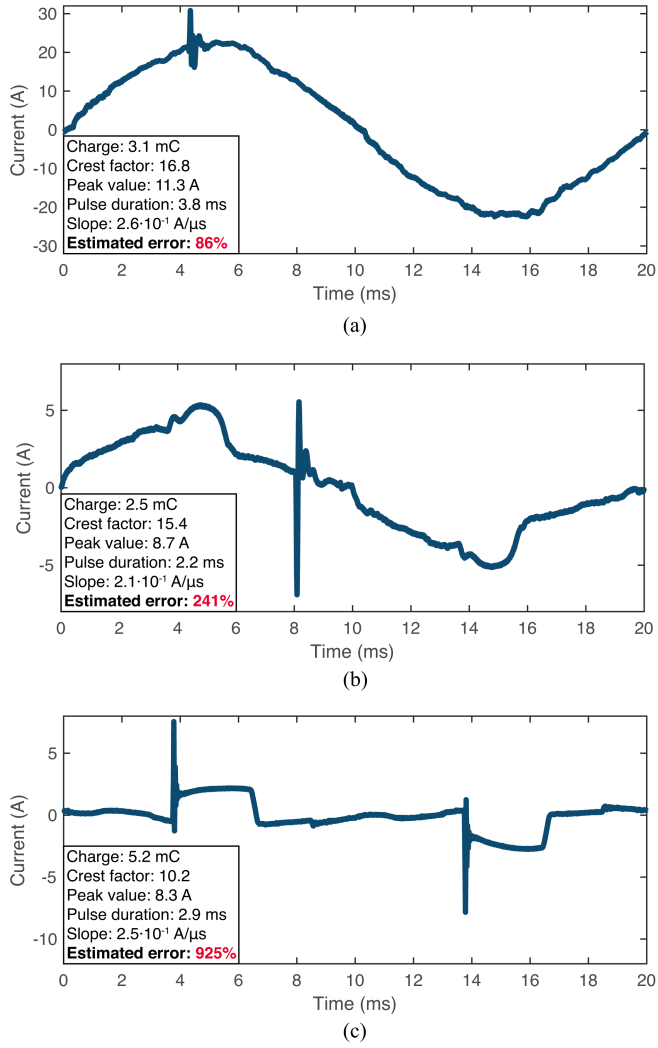

Fig. 8. Waveforms with an estimated static energy meter error surveyed in the sites. (a) Site 1. (b) Site 2. (c) Site 3.

C. Test Site 3

For site 3, a total of 4006 events were captured, of which 779 contain critical parameters, and for 332, an error was estimated. This is mostly because of the high crest factor and high rising slope found in these waveforms. A waveform for which an error was estimated is exemplified in Fig. 8(c); the interference repeats during multiple consecutive cycles. It shows a pulsed current waveform without a clear sinusoidal component present; this represents a similar situation as the pulses causing static energy meter interference in laboratory experiments. During the ten-day survey in site 3, similar pulses were identified five times during intervals of 1.5–3 h. This indicates that the pulse is resulting from the equipment that is not running continuously; however, the pulses occurred during different times of the day. The estimated errors for site 3 range from −35% to 925%. The variation of the estimated error mainly occurs due to a difference in the crest factor and the rising slope between different occurrences of the event.

VI. Discussion

In this article, waveforms likely to be critical in relation with static energy meter interference are detected in on-site surveyed waveforms. This is done using a parametric waveform model for the characterization of pulses in on-site scenarios. Then, a dataset of laboratory experiments, of which static energy meter errors are known, is interpolated to the unknown surveyed waveforms using an IDW function to estimate the interference. As a result, surveyed waveform data with similar characteristics are detected. These detected waveforms show the existence of several waveforms in on-site situations that have similar characteristics as the waveforms proven to result in static energy meter interference. In 74% of the surveyed waveforms, parameters in the critical range were found. The estimated errors range from -35% to 925% depending on the extremity of the time-domain parameters of the pulse. Furthermore, the presented parameters in the on-site data show that, in general, a variety of nonlinear waveforms are present in LV networks and are thus encountered by the static energy meters. These nonlinearities are outside the requirements as included in immunity standards such as the IEC 61000-4-19 [7]. This can become problematic as equipment inside such systems, e.g., the static energy meter, is characterized using frequency-domain tests. These tests are only valid if the system can be considered as linear time invariant; however, this is clearly not the case, as was already pointed out in [27].

VII. Conclusion

Several waveforms that are nonlinear and have a highly pulsed character are found to exist in on-site surveyed data. These have similar time-domain parameters to waveforms that are proven to result in static energy meter interference and are thus likely to cause similar errors. This was verified using an estimator that interpolates the on-site data with respect to a reference dataset containing waveforms that induced meter errors, based on an IDW function, such that pulses with similar characteristics are detected. For 74% of the surveyed waveforms, parameters inside the critical range related to static energy meter interference were found. The existence of these nonlinearities in on-site waveforms shows that on-site systems contain more nonlinearities than immunity standards as the IEC 61000-4-19 envision. As a result, problems in LV systems may arise, for example, EMI of static energy meters.

References

[1] A. Cataliotti, V. Cosentino, and S. Nuccio, "Static meters for the reactive energy in the presence of harmonics: An experimental metrological characterization," *IEEE Trans. Instrum. Meas.*, vol. 58, no. 8, pp. 2574–2579, Aug. 2009.

[2] J. Kirchhof and G. Klein, "EMV—Grenzwertlücke—Wechselrichter stört Zähler," in *Proc. 24th Symp. Photovolt. Sol. Energy*, Bad Staffelstein, Germany, 2009, pp. 1–8.

[3] J. Kirchhof, "Grenzwertlücke—Wechselrichter stört elektrizitätszähler," in *Proc. Int. Fachmesse und Kongress Elektromagn. Verträglichkeit*, Düsseldorf, Germany, 2010, pp. 1–9.

[4] R. B. Timens, "Electromagnetic interference of equipment in power supply networks," Ph.D. dissertation, Univ. Twente, Enschede, The Netherlands, 2013.

[5] CENELEC, "Study report on electromagnetic interference between electrical equipment/systems in the frequency range below 150 kHz," CENELEC, Brussels, Belgium, Tech. Rep. CLC/TR 50627, 2014.

[6] CENELEC "Electricity metering equipment—Severity levels, immunity requirements and test methods for conducted disturbances in the frequency range 2 -150 kHz," CENELEC, Brussels, Belgium, Tech. Rep. CLC/TR 50579, 2012.

[7] *Electromagnetic Compatibility (EMC)—Part 4-19: Testing and Measurement Techniques—Test for Immunity to Conducted, Differential Mode Disturbances and Signalling in the Frequency Range from 2 kHz to 150 kHz, at A.C. Power Port*, *IEC Standard IEC 61000-4-19*, 2014.

[8] F. Leferink, C. Keyer, and A. Melentjev, "Static energy meter errors caused by conducted electromagnetic interference," *IEEE Electromagn. Compat. Mag.*, vol. 5, no. 4, pp. 49–55, Oct.–Dec. 2016.

[9] Z. Marais, H. E. Van den Brom, G. Rietveld, R. Van Leeuwen, D. Hoogenboom, and J. Rens, "Sensitivity of static energy meter reading errors to changes in non-sinusoidal load conditions," in *Proc. Int. Symp. Electromagn. Compat.*, Barcelona, Spain, 2019, pp. 202–207.

[10] B. ten Have, T. Hartman, N. Moonen, and F. Leferink, "Inclination of fast changing currents effect the readings of static energy meters," in *Proc. Int. Symp. Electromagn. Compat.*, Barcelona, Spain, 2019, pp. 208–213.

[11] B. ten Have, T. Hartman, N. Moonen, C. Keyer, and F. Leferink, "Faulty readings of static energy meters caused by conducted electromagnetic interference from a water pump," *Renewable Energy Power Qual. J.*, Santa Cruz de Tenerife, Spain, vol. 17, pp. 15–19, 2019.

[12] B. ten Have, T. Hartman, N. Moonen, and F. Leferink, "Misreadings of static energy meters due to conducted EMI caused by fast changing current," in *Proc. Joint Int. Symp. Electromagn. Compat./Asia-Pacific Int. Symp. Electromagn. Compat.*, Sapporo, Japan, 2019, pp. 445–448.

[13] R. Quijano Cetina, Y. Seferi, S. M. Blair, and P. S. Wright, "Energy metering integrated circuit behavior beyond standards requirements," *Energies*, vol. 14, no. 2, pp. 1–19, Jan. 2021.

[14] B. ten Have *et al.*, "Waveform model to characterize time-domain pulses resulting in EMI on static energy meters," *IEEE Trans. Electromagn. Compat.*, early access, Apr. 9, 2021, doi: 10.1109/TEMC.2021.3062948

[15] P. Jaques, R. Kolander, R. Hartig, R. Stiegler, A. Fröbel, and J. Meyer, "Survey of current gradient at public low voltage customer terminals in Germany," in *Proc. 25th Int. Conf. Elect. Distrib.*, Madrid, Spain, 2019, pp. 1–5.

[16] "Electromagnetic interference on static electricity meters," EURAMET e.V., Braunschweig Germany, MeterEMI Project 17NRM02,, 2019.

[17] T. Hartman, M. Pous, M. A. Azpúrua, F. Silva, and F. Leferink, "On-site waveform characterization at static meters loaded with electrical vehicle chargers," in *Proc. Int. Symp. Electromagn. Compat.*, Barcelona, Spain, 2019, pp. 191–196.

[18] B. ten Have, M. A. Azpúrua, M. Pous, F. Silva, and F. Leferink, "On-site waveform survey in LV distribution network using a photovoltaic installation," in *Proc. Int. Symp. Electromagn. Compat.*, Rome, Italy, 2020, pp. 1–6.

[19] *IEEE Standard for Transitions, Pulses, and Related Waveforms*, IEEE Standard 181–2011 (*Revision of IEEE Standard 181-2003)*, 2011.

[20] M. A. Azpúrua and K. D. Ramos, "A comparison of spatial interpolation methods for estimation of average electromagnetic field magnitude," *Prog. Electromagn. Res.*, vol. 14, pp. 135–145, 2010.

[21] *Electricity Metering Equipment (A.C.)—Part 3: Particular Requirements—Static Meters for Active Energy (Class Indexes A, B and C)*, European Standard EN 50470-3, 2006.

[22] B. ten Have, N. Moonen, and F. Leferink, "Time domain analysis of current transducer responses using impulsive signals," *IEEE Lett. Electromagn. Compat. Pract. Appl.*, vol. 3, no. 1, pp. 19–23, Mar. 2021.

[23] M. A. Azpúrua, M. Pous, J. A. Oliva, B. Pinter, M. Hudlicka, and F. Silva, "Waveform approach for assessing conformity of CISPR 16-1-1 measuring receivers," *IEEE Trans. Instrum. Meas.*, vol. 67, no. 5, pp. 1187–1198, May 2018.

[24] M. Pous, M. A. Azpúrua, and F. Silva, "APD oudoors time-domain measurements for impulsive noise characterization," in *Proc. Int. Symp. Electromagn. Compat.*, Angers, France, 2017, pp. 1–6.

[25] F. Barakou, P. S. Wright, H. E. van den Brom, G. Kok, and G. Rietveld, "Detection methods for current signals causing errors in static electricity meters," in *Proc. Int. Symp. Electromagn. Compat.*, Barcelona, Spain, 2019, pp. 273–278.

[26] H. Wickham and L. Stryjewski, "40 years of boxplots," 2012.

[27] B. ten Have, T. Hartman, N. Moonen, and F. Leferink, "Why frequency domain tests like IEC 61000-4-19 are not valid; a call for time domain testing," in *Proc. Int. Symp. Electromagn. Compat.*, Barcelona, Spain, 2019, pp. 124–128.

Bas ten Have (Student Member, IEEE) received the B.Sc. and M.Sc. degrees in electrical engineering in 2015 and 2018, respectively, both from the University of Twente, Enschede, The Netherlands, where he is currently working toward the Ph.D. degree in electromagnetic compatibility with the Power Electronics and Electromagnetic Compatibility Group.

His research interests include sustainable, energy-efficient, innovations of products, systems and applications, low-frequency electromagnetic interference, power systems, power electronics, and smart grids.

Marco A. Azpúrua (Senior Member, IEEE) received the B.Sc. degree in telecommunications engineering and the M.Sc. degree in electrical engineering from the Universidad Central de Venezuela, Caracas, Venezuela, in 2008 and 2013, respectively, and the Ph.D. degree in electronics engineering from the Universitat Politécnica de Catalunya (UPC), Barcelona, Spain, in 2018.

He is currently a Researcher with the Electromagnetic Compatibility Group, UPC. He is the Co-founder of EMC Barcelona, Barcelona. Previously, he was a Researcher with the Applied Electromagnetics Laboratory, Fundación Instituto de Ingeniería, Caracas, Venezuela. His research interests include electromagnetic compatibility, estimation of measurement uncertainty, and validation methods.

Dr. Azúrua is a member of the IEEE Electromagnetic Compatibility Society, the IEEE Instrumentation and Measurement Society, and the International Committee on Electromagnetic Safety. He was a recipient of the IEEE Instrumentation and Measurement Society Faculty Course Development Award in 2020 and the Best Symposium Student Paper Award at the Electromagnetic Compatibility Europe International Symposium on Electromagnetic Compatibility in 2017.

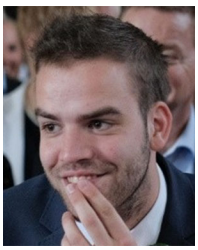

Tom Hartman (Student Member, IEEE) received the bachelor's degree in electrical engineering from the University of Twente, Enschede, The Netherlands, in 2016, and the master's degree in electrical engineering in 2018 from the Group of Telecommunication Engineering, University of Twente, where he is currently working toward the Ph.D. degree in electromagnetic compatibility with the Power Electronics and Electromagnetic Compatibility Group.

He is working on a project about electromagnetic interference on static electricity meters, in which he works on improving the digital signal processing techniques used for multichannel time-domain electromagnetic interference measurements.

Marc Pous (Member, IEEE) received the M.Sc. degree in telecommunications engineering and the Ph.D. degree in electronics engineering from the Universitat Politécnica de Catalunya, Barcelona, Spain, in 2009 and 2015, respectively.

From 2003 to 2006, he was with the Department of Electromagnetic Compatibility, LGAI Technological Centre, Barcelona. In 2006, he joined the Electromagnetic Compatibility Group, Universitat Politécnica de Catalunya, where he is currently conducting his research. He is also Co-Founder of EMC Barcelona startup being the Business Manager of the company. He has been participating in international and national research projects related to the automotive, aerospace, railway, and medical industries. His research interests include the development of novel time-domain interference measurement techniques and new evaluation methods to overcome not properly measured disturbances following the harmonized electromagnetic compatibility standards.

Dr. Pous is a member of the International Steering Committee EMC Europe, the Vice-Chairman of Electromagnetic Compatibility Europe 2019, Barcelona, and the Treasurer of the IEEE Electromagnetic Compatibility Society Spanish chapter.

Niek Moonen (Member, IEEE) received the B.Sc. degree in advanced technology, the M.Sc. degree in electrical engineering, and the Ph.D. (*cum laude*) degree in electromagnetic compatibility from the University of Twente, Enschede, The Netherlands, in 2012, 2014, and 2019, respectively.

Since January 2019, he has been an Assistant Professor with the Power Electronics and Electromagnetic Compatibility Group, University of Twente. His research interests include electromagnetic interference (EMI) mitigation in power electronics with special interest in EMI propagation in smart grids, digital signal processing in electromagnetic compatibility measurements, and EMI filter optimization.

Dr. Moonen is a member of the IEEE Electromagnetic Compatibility Society TC7 on low-frequency electromagnetic compatibility and a Board Member of the Dutch EMC-ESD Association.

Ferran Silva (Senior Member, IEEE) received the M.Sc. and Ph.D. degrees in telecommunication engineering from the Universitat Politécnica de Catalunya (UPC), Barcelona, Spain, in 1989 and 1997, respectively.

He is currently an Associate Professor in electronics with the Department of Electronic Engineering, UPC. Since 1993, he has been the Head of the Electromagnetic Compatibility Group, UPC. He is the author of more than 140 publications about electromagnetic compatibility (EMC) in journals, conferences, and books. Since 1993, he has participated in 32 research projects related to EMC. His research interests include EMC in near field and time domain, with application to transport, medical, and industrial areas.

Dr. Silva is a senior member of the IEEE EMC Society, where he is the Head of the Spanish chapter in two different periods. He is also a member of the EMC Spanish Standardization Committees SCTC77-210 and the CTN208 SCCISPR210A. He was the Chairman of the EMC Europe International Symposium editions in Barcelona in 2006 and 2019. Since 2004, he has been a member of the EMC Europe International Steering Committee.

Frank Leferink (Fellow, IEEE) received the B.Sc., M.Sc., and Ph.D. degrees in electrical engineering from the University of Twente, Enschede, The Netherlands, in 1984, 1992, and 2001, respectively.

Since 1984, he has been with Thales Nederland B.V., Hengelo, The Netherlands, where he is the Director Electromagnetic Compatibility (EMC) and a Manager of the Network of Excellence on EMC, with more than 100 EMC engineers scattered over more than 20 units, worldwide. In 2003, he joined as (part-time, full research) Professor and holds the Chair for EMC with the University of Twente. He has authored and coauthored more than 300 papers published in international conferences or peer-reviewed journals. He holds five patents.

Dr. Leferink is the Past President of the Dutch EMC-ESD Association, the Chair of the IEEE EMC Benelux Chapter, a member of the International Steering Committee of the EMC Europe, the Chairman of the EMC Europe 2018, Amsterdam, The Netherlands, and a member of the Board of Directors of the IEEE EMC Society. He is an Associate Editor for the IEEE TRANSACTIONS ON ELECTROMAGNETIC COMPATIBILITY and IEEE LETTERS ON ELECTROMAGNETIC COMPATIBILITY PRACTICE AND APPLICATIONS.